

## Method for detecting subtle spatial structures by fluctuation microscopy

Toshiya Iwai

*Department of Applied Physics, Tohoku University, Sendai 980-8579, Japan  
and Department of Physics, University of Illinois at Urbana-Champaign, 1110 West Green Street, Urbana, Illinois 61801*

P. M. Voyles, J. Murray Gibson, and Yoshitsugu Oono

*Department of Physics, University of Illinois at Urbana-Champaign, 1110 West Green Street, Urbana, Illinois 61801*

(Received 15 January 1999; revised manuscript received 10 March 1999)

Subtle spatial structures are often reflected on higher-order correlations. Fluctuation microscopy is a good method for detecting such spatial structures in disordered materials, because the method detects the contribution of the fourth-order density distribution function. We propose an improvement for fluctuation microscopy that increases its sensitivity to subtle spatial structures by enhancing the contributions of both the third- and the fourth-order density cumulant functions to the observable. We demonstrate numerically that the proposed method provides better detection of subtle structural changes than the original approach with improved stability against experimental noise. Although we illustrate the method in terms of transmission electron microscopy, it is not confined to this microscopy. [S0163-1829(99)07925-4]

### I. INTRODUCTION

Pair-correlation functions obtained from diffraction experiments have been the most popular means to study spatial structure quantitatively. However, needless to say, not all the structural features can be captured by the second moment of the density distribution. For example, it is impossible to obtain the distribution of the curvature of interfaces from the pair-correlation function alone. Furthermore, subtle spatial structural changes are more often reflected on higher-order correlation functions than the pair-correlation function. Therefore, it is desirable to devise experimental techniques that allow us to capture some aspects of correlation functions of higher order than the pair-correlation function.

Recently, Treacy and Gibson<sup>1</sup> demonstrated a method to detect subtle spatial structural changes through variable coherence transmission electron microscopy (TEM), a form of fluctuation microscopy. They introduced the normalized speckle variance (NSV), obtained from the mean and the second moment of the kinematical coherent dark-field-image intensity. Gibson and Treacy<sup>2,3</sup> studied the annealing process of amorphous germanium with the NSV and successfully detected structural changes that were hardly observable in the mean intensity (i.e., the pair-correlation function of the density). The sensitivity of the NSV is due to the higher-order correlation function contributions captured in the second moment of the dark-field-image intensity.

There have been efforts to extract more information from diffraction experiments than the usual form factor and the two-body correlation function. For example, critical dynamics in Fe<sub>3</sub>Al and the equilibrium dynamics of block copolymer have been observed by x-ray intensity fluctuation spectroscopy,<sup>4,5</sup> and the Brownian motion of colloidal particles in fluids has been observed by x-ray photon correlation spectroscopy.<sup>6,7</sup> Numerical studies of scattering speckle from

phase ordering systems have demonstrated a scaling property of the two-time correlation function.<sup>8</sup>

However, these speckle-related studies do not pay any attention to the contribution of higher-order density correlations in the sample, which were the object of the effort by Gibson and Treacy. It is natural to attempt to improve their approach by subtracting the lower-order distribution functions as completely as possible from the second moment of the kinematical coherent dark-field-image intensity in order to further accentuate subtle structural changes. We thus propose a quantity, the higher-order speckle cumulant (HSC), which maximally removes the contribution of the two-body correlation function. We demonstrate the power of the HSC in detecting subtle structural changes with numerical experiments. The HSC changes more systematically with the magnitude of changes to the structure than the NSV in our numerical experiments. We have also found that our proposed quantity is more stable against experimental noise than the NSV.

Fluctuation microscopy depends on microscopic imaging with diffracted radiation. The most readily available experimental realization of the HSC is dark-field TEM imaging. Thus, our explanation closely follows the TEM practice. However, the basic theory of diffraction from disordered materials and wave optics could be applied to other systems, such as the biaxial liquid crystal studied through light-scattering experiments. Moreover, although we restrict ourselves to two-dimensional samples in this paper for our numerical demonstration, the HSC should be applicable to bulk materials of disordered systems that may be studied with the aid of, e.g., neutron-scattering experiments.

In Sec. II, we briefly explain the TEM imaging terminology and introduce the HSC and its empirical object (eHSC). A practical procedure to compute the eHSC from a TEM image is summarized in Sec. III. In Sec. IV, we demonstrate the power of the NSV and especially the eHSC in detecting subtle structural changes. Section V is a summary.

## II. METHOD TO DETECT SUBTLE SPATIAL STRUCTURES

The wave function  $U(\vec{K}, \vec{R})$  for kinematical coherent dark-field imaging in a TEM can be shown to be<sup>9</sup>

$$U(\vec{K}, \vec{R}) = \phi(\vec{K}) \int d\vec{R}' A(\vec{R} - \vec{R}') \psi(\vec{R}') e^{-i\vec{k} \cdot \vec{R}'}, \quad (2.1)$$

where  $\vec{R}$  is a position vector in the image, and  $\vec{K}$  is the average scattering vector accepted by the objective aperture.  $\psi$  is the atomic density function that is defined over the specimen and  $\phi(\vec{K})$  is the atomic scattering factor. The function  $A$  is the Fourier transform of the aperture function and is given by

$$A(\vec{R}) = \int_{|\vec{q}| < Q} d\vec{q} e^{i\vec{q} \cdot \vec{R}}, \quad (2.2)$$

where  $Q$  is the radius of the objective aperture in reciprocal space and  $\vec{q}$  is a two-dimensional vector in the objective aperture plane in reciprocal space. The TEM image is, of course, the intensity  $|U(\vec{R}, \vec{K})|^2$ .

In the case of a two-dimensional specimen (which we use here as an approximation for real, thin samples), both  $\vec{K}$  and  $\vec{R}$  can be replaced by two-dimensional vectors  $\vec{k}$  and  $\vec{r}$  that lie in the specimen, because  $\vec{R} - \vec{R}'$  in Eq. (2.1) is a two-dimensional vector. The explicit expression for  $A(\vec{r})$  is given in terms of the Bessel function  $J_1$ ,

$$A(\vec{r}) = \pi Q^2 \frac{2J_1(Q|\vec{r}|)}{Q|\vec{r}|}. \quad (2.3)$$

Averaging over both the image area and an ensemble of structures, we obtain the mean coherent dark-field-image intensity as

$$\langle\langle I(\vec{k}) \rangle\rangle = \frac{1}{S} \int d\vec{r} \langle |U(\vec{k}, \vec{r})|^2 \rangle_e \quad (2.4)$$

$$= \frac{|\phi(\vec{k})|^2}{S} \int d\vec{r} \int d\vec{r}_1 \int d\vec{r}_2 A(\vec{r} - \vec{r}_1) \times A(\vec{r} - \vec{r}_2) \rho_2(\vec{r}_1, \vec{r}_2) e^{i\vec{k} \cdot (\vec{r}_1 - \vec{r}_2)}, \quad (2.5)$$

where double brackets mean both spatial and ensemble averages, single brackets with a subscript  $e$  mean ensemble average,  $\rho_2(\vec{r}, \vec{r}') = \langle \psi(\vec{r}) \psi(\vec{r}') \rangle_e$  is the two-body distribution function, and  $S$  is the area of the two-dimensional specimen. We also consider the second moment of the image intensity,

$$\langle\langle I^2(\vec{k}) \rangle\rangle = \frac{1}{S} \int d\vec{r} \langle |U(\vec{k}, \vec{r})|^4 \rangle_e \quad (2.6)$$

$$= \frac{|\phi(\vec{k})|^4}{S} \int d\vec{r} \prod_{j=1}^4 \left\{ \int d\vec{r}_j A(\vec{r} - \vec{r}_j) \right\} \times \rho_4(\vec{r}_1, \vec{r}_2, \vec{r}_3, \vec{r}_4) e^{i\vec{k} \cdot (\vec{r}_1 - \vec{r}_2 + \vec{r}_3 - \vec{r}_4)}, \quad (2.7)$$

where  $\rho_4(\vec{r}_1, \vec{r}_2, \vec{r}_3, \vec{r}_4) = \langle \psi(\vec{r}_1) \psi(\vec{r}_2) \psi(\vec{r}_3) \psi(\vec{r}_4) \rangle_e$  is the four-body distribution function.

The NSV is defined as

$$\langle\langle V(\vec{k}) \rangle\rangle = \frac{\langle\langle I^2(\vec{k}) \rangle\rangle}{\langle\langle I(\vec{k}) \rangle\rangle^2}. \quad (2.8)$$

We need no more than the image intensities  $|U(\vec{k}, \vec{r})|^2$  to get the NSV. This quantity was previously used by Gibson and Treacy. Their definition is the same as above except for the subtraction of 1. Since the function  $A$  is extremely localized, spatial averaging is assumed to play the roles of both spatial and ensemble averaging.

In order to extract higher-order spatial correlations, we subtract the lower-order correlation terms, which can be constructed from the average density and the two-body distribution function, from  $\langle\langle I^2(\vec{k}) \rangle\rangle$  with the aid of the cumulant expansion:<sup>10</sup>

$$\begin{aligned} \rho_4(\vec{r}_1, \vec{r}_2, \vec{r}_3, \vec{r}_4) &= c_4(\vec{r}_1, \vec{r}_2, \vec{r}_3, \vec{r}_4) + \rho_1(r_1) c_3(\vec{r}_2, \vec{r}_3, \vec{r}_4) \\ &\quad + \rho_1(r_2) c_3(\vec{r}_1, \vec{r}_3, \vec{r}_4) \\ &\quad + \rho_1(r_3) c_3(\vec{r}_1, \vec{r}_2, \vec{r}_4) \\ &\quad + \rho_1(r_4) c_3(\vec{r}_1, \vec{r}_2, \vec{r}_3) \\ &\quad + \rho_2(\vec{r}_1, \vec{r}_2) \rho_2(\vec{r}_3, \vec{r}_4) \\ &\quad + \rho_2(\vec{r}_1, \vec{r}_3) \rho_2(\vec{r}_2, \vec{r}_4) \\ &\quad + \rho_2(\vec{r}_1, \vec{r}_4) \rho_2(\vec{r}_2, \vec{r}_3) \\ &\quad - 2\rho_1(\vec{r}_1) \rho_1(\vec{r}_2) \rho_1(\vec{r}_3) \rho_1(\vec{r}_4), \end{aligned} \quad (2.9)$$

where  $c_4(\vec{r}_1, \vec{r}_2, \vec{r}_3, \vec{r}_4)$ ,  $c_3(\vec{r}_1, \vec{r}_2, \vec{r}_3)$  and  $\rho_1(\vec{r}_1)$  are the four-body cumulant function, the three-body cumulant function and the density, respectively. In Eq. (2.9), the two-body distribution function  $\rho_2$  is used instead of the two-body cumulant function for later convenience. Substituting Eq. (2.9) into Eq. (2.7) gives terms that depend only on lower-order correlations (two-body and the density), which we group together as  $\langle\langle I^2 \rangle\rangle_L$ , and terms that depend only on higher-order correlations (three- and four-body), which we group together as  $\langle\langle I^2 \rangle\rangle_H$

$$\langle\langle I^2(\vec{k}) \rangle\rangle_H = \langle\langle I^2(\vec{k}) \rangle\rangle - \langle\langle I^2(\vec{k}) \rangle\rangle_L. \quad (2.10)$$

$$\begin{aligned} \langle\langle I^2(\vec{k}) \rangle\rangle_L &= \frac{2|\phi(\vec{k})|^4}{S} \int d\vec{r} \left\{ \int d\vec{r}_1 \int d\vec{r}_2 A(\vec{r}-\vec{r}_1) \right. \\ &\quad \times A(\vec{r}-\vec{r}_2) \rho_2(\vec{r}_1, \vec{r}_2) e^{i\vec{k}\cdot(\vec{r}_1-\vec{r}_2)} \left. \right\}^2 \\ &\quad + \frac{|\phi(\vec{k})|^4}{S} \int d\vec{r} \left| \int d\vec{r}_1 \int d\vec{r}_2 A(\vec{r}-\vec{r}_1) \right. \\ &\quad \times A(\vec{r}-\vec{r}_2) \rho_2(\vec{r}_1, \vec{r}_2) e^{i\vec{k}\cdot(\vec{r}_1+\vec{r}_2)} \left. \right|^2 \\ &\quad - \frac{2|\phi(\vec{k})|^4}{S} \int d\vec{r} \left| \int d\vec{r}_1 A(\vec{r}-\vec{r}_1) \rho_1(\vec{r}_1) e^{i\vec{k}\cdot\vec{r}_1} \right|^4 \end{aligned} \quad (2.11)$$

$$= \frac{1}{S} \int d\vec{r} \{ 2\langle |U(\vec{k}, \vec{r})|^2 \rangle_e^2 + |\langle U(\vec{k}, \vec{r})^2 \rangle_e|^2 - 2|\langle U(\vec{k}, \vec{r}) \rangle_e|^4 \}. \quad (2.12)$$

We introduce a new quantity different from the NSV, the HSC, defined by

$$\langle\langle H(\vec{k}) \rangle\rangle = \frac{\langle\langle I^2(\vec{k}) \rangle\rangle_H}{\langle\langle I^2(\vec{k}) \rangle\rangle_L}. \quad (2.13)$$

Let us consider the measurement of  $\langle\langle I^2 \rangle\rangle_H$ . Single experiment in the TEM yields the image intensity  $|U(\vec{k}, \vec{r})|^2$ . The first term on the right-hand side of Eq. (2.10) is measurable (as is the NSV). The first term in Eq. (2.12) is also measurable directly from the image, but the second and third terms are not. Equation (2.11) shows that the third term can be calculated from the density  $\rho_1$ , which is measurable in a TEM. That leaves the second term in Eq. (2.12), which depends on the two-body distribution function  $\rho_2$ .  $\rho_2$  can be measured from the diffraction pattern in a TEM, but that requires a separate measurement from the image, with the attendant uncertainties. It would be preferable to calculate  $\langle\langle I^2 \rangle\rangle_L$  completely from one image. The second term can be calculated from  $\langle\langle I \rangle\rangle$ , if  $\rho_2(\vec{r}, \vec{r}')$  is assumed as a function of  $\vec{r}-\vec{r}'$ ,

$$\rho_2(\vec{r}, \vec{r}') = \rho_2(\vec{r}-\vec{r}'). \quad (2.14)$$

We will call the HSC obtained with this approximation empirical HSC (eHSC). Practitioners need not read the rest of this section, and can go to the practical procedure summarized in the next section.

To simplify the calculation and to remove ambiguity in the normalization, we assume real space and reciprocal space

are both discrete. Due to the finite resolution of the actual imaging this should not cause any fundamental problems. We assume that space is an  $N \times N$  ‘‘fictitious’’ lattice. We introduce discrete vectors  $\vec{X} = (\vec{r} + \vec{r}')/2$  and  $\vec{R} = \vec{r} - \vec{r}'$  to describe  $\vec{r}$  and  $\vec{r}'$ .  $R_\alpha$ , the  $\alpha$  component of  $\vec{R}$ , takes values  $j \times a$  ( $j = -N+1, -N+2, \dots, N-1$ ) and similarly  $X_\alpha = j \times a + \frac{1}{2}|R_\alpha|$  ( $j = 1, 2, \dots, N$ ), where  $\alpha = x, y$  and  $a$  is the ‘‘lattice spacing’’ of the underlying fictitious lattice.  $\langle\langle I \rangle\rangle$ ,  $\langle\langle I^2 \rangle\rangle$ , and  $\langle\langle I^2 \rangle\rangle_L$  are understood as sampled values at the underlying fictitious lattice (the sampling lattice). Thus, introduction of the fictitious lattice corresponds to the actual data acquisition.  $\langle |U|^{2n} \rangle_e$  in Eqs. (2.4), (2.6), and (2.12) is understood as a discrete Fourier transformation given by

$$\begin{aligned} \langle |U(\vec{k}, \vec{j}a)|^{2n} \rangle_e &= \frac{1}{N^{2n}} \prod_{\nu=1}^n \left\{ \sum_{\vec{j}_{2\nu-1}} \sum_{\vec{j}_{2\nu}} A(\vec{j}a - \vec{j}_{2\nu-1}a) \right. \\ &\quad \times A(\vec{j}a - \vec{j}_{2\nu}a) e^{i\vec{k}\cdot(\vec{j}_{2\nu-1} - \vec{j}_{2\nu})a} \left. \right\} \\ &\quad \times \rho_{2n}(\vec{j}_1a, \vec{j}_2a, \dots, \vec{j}_{2n-1}a, \vec{j}_{2n}a) \\ &= \mathcal{F}[\vec{j}_1a, \vec{k}] \{ \mathcal{F}[\vec{j}_2a, -\vec{k}] \\ &\quad \times \{ \dots \mathcal{F}[\vec{j}_{2n-1}a, \vec{k}] \{ \mathcal{F}[\vec{j}_{2n}a, -\vec{k}] \\ &\quad \times \{ A(\vec{j}a - \vec{j}_1a) A(\vec{j}a - \vec{j}_2a) \dots \\ &\quad \times A(\vec{j}a - \vec{j}_{2n-1}a) A(\vec{j}a - \vec{j}_{2n}a) \\ &\quad \times \rho_{2n}(\vec{j}_1a, \vec{j}_2a, \dots, \vec{j}_{2n-1}a, \vec{j}_{2n}a) \} \dots \} \}, \end{aligned} \quad (2.15)$$

where the two-dimensional discrete Fourier transformation is denoted by  $\mathcal{F}[\vec{j}, \vec{k}] \{ \dots \}$  and defined as

$$\mathcal{F}[\vec{j}a, \vec{k}] \{ f(\vec{j}a) \} = \frac{1}{N} \sum_{j_x=1}^N \sum_{j_y=1}^N f(\vec{j}a) e^{i\vec{k}\cdot\vec{j}a}, \quad (2.16)$$

where the  $\alpha$  component of  $\vec{k}$  equals  $2\pi\vec{k}_\alpha/(Na)$  [ $\vec{k}_\alpha = 1, 2, \dots, N$  ( $\alpha = x, y$ )]. This definition of the discrete Fourier transformation of  $\langle |U|^{2n} \rangle_e$  includes the normalization factor  $1/N^{2n}$ . Since both numerator and denominator in Eqs. (2.8) and (2.13) contain the same power of  $U$ , the normalization factor does not affect the magnitude of either the NSV or HSC. Spatial integration over the variable  $\vec{r}$  in Eqs. (2.4), (2.6), and (2.12) is replaced by the summation over the sampling points with the volume element  $dx^2 = a^2$ .

In order to compute  $\rho_2$  from  $\langle\langle I(\vec{k}) \rangle\rangle$ , discrete inverse Fourier transformation of  $\langle\langle I(\vec{k}) \rangle\rangle$  is defined as follows from Eqs. (2.5) and (2.16):

$$\begin{aligned}
\mathcal{F}^{-1}[\vec{z}, \vec{k}]\{\langle\langle I(\vec{k}) \rangle\rangle\} &= \frac{1}{N} \sum_{\vec{k}} \langle\langle I(\vec{k}) \rangle\rangle e^{-i\vec{k} \cdot \vec{z}} \\
&= \frac{a^2}{NS} \sum_{\vec{k}} \sum_{\vec{j}a} \langle |U(\vec{k}, \vec{j}a)|^2 \rangle e^{-i\vec{k} \cdot \vec{z}} \\
&= \frac{1}{N^3} \sum_{\vec{k}} \sum_{\vec{j}a} \frac{|\phi(\vec{k})|^2}{N^2} \sum_{\vec{j}_1a} \sum_{\vec{j}_2a} A(\vec{j}a - \vec{j}_1a) A(\vec{j}a - \vec{j}_2a) \rho_2(\vec{j}_1a - \vec{j}_2a) \exp\{i\vec{k} \cdot (\vec{j}_1a - \vec{j}_2a - \vec{z})\} \\
&= \frac{|\phi(\vec{k})|^2}{N^5} \prod_{\alpha=x,y} \left\{ \sum_{\vec{k}_\alpha=1}^N \sum_{R_\alpha/a=-N+1}^{N-1} \sum_{X_\alpha/a=1+|R_\alpha|/(2a)}^{L-|R_\alpha|/(2a)} \right\} \\
&\quad \times \sum_{\vec{j}} A(\vec{j}a - \vec{X} - \vec{R}/2) A(\vec{j}a - \vec{X} + \vec{R}/2) \rho_2(\vec{R}) \exp\{i\vec{k} \cdot (\vec{R} - \vec{z})\}, \tag{2.17}
\end{aligned}$$

where the  $\alpha$  component of  $\vec{z}$  takes  $a, 2a, \dots, Na$  ( $\alpha=x, y$ ),  $\vec{R} = \vec{j}_1a - \vec{j}_2a$ ,  $\vec{X} = (\vec{j}_1a + \vec{j}_2a)/2$ , and volume element divided by the area  $a^2/S$  is equal to  $1/N^2$ . The function  $A$  defined by Eq. (2.2) satisfies the following equation with  $\vec{r}$  a continuous variable:

$$\int_{-\infty}^{\infty} \int_{-\infty}^{\infty} d\vec{r} A(\vec{r} - \vec{Y}_1) A(\vec{r} - \vec{Y}_2) = A(\vec{Y}_1 - \vec{Y}_2). \tag{2.18}$$

In the case of discrete variables, we define a function  $A_2$  such that

$$A_2(\vec{Y}_1 - \vec{Y}_2) = \sum_{j_x=1}^N \sum_{j_y=1}^N A(\vec{j}a - \vec{Y}_1) A(\vec{j}a - \vec{Y}_2). \tag{2.19}$$

We may approximate  $A_2$  as a function of  $\vec{Y}_1 - \vec{Y}_2$  only, which has been confirmed numerically. Using Eq. (2.19), Eq. (2.17) becomes

$$\begin{aligned}
\mathcal{F}^{-1}[\vec{z}, \vec{k}]\{\langle\langle I(\vec{k}) \rangle\rangle\} &= \frac{|\phi(\vec{k})|^2}{N^5} \prod_{\alpha=x,y} \left\{ \sum_{\vec{k}_\alpha} \sum_{R_\alpha/a=-N+1}^{N-1} \sum_{X_\alpha/a=1+|R_\alpha|/(2a)}^{N-|R_\alpha|/(2a)} \right\} A_2(\vec{R}) \rho_2(\vec{R}) \exp\{i\vec{k} \cdot (\vec{R} - \vec{z})\} \\
&= \frac{|\phi(\vec{k})|^2}{N^5} \prod_{\alpha=x,y} \left\{ \sum_{\vec{k}_\alpha} \sum_{R_\alpha} \left( N - \frac{|R_\alpha|}{a} \right) \right\} A_2(\vec{R}) \rho_2(\vec{R}) \exp\{i\vec{k} \cdot (\vec{R} - \vec{z})\} \\
&= \frac{|\phi(\vec{k})|^2}{N^3} \left\{ \left( N - \frac{z_x}{a} \right) \left( N - \frac{z_y}{a} \right) A_2(z_x, z_y) \rho_2(z_x, z_y) + \left( N - \frac{z_x}{a} \right) \frac{z_y}{a} A_2(z_x, Na - z_y) \rho_2(z_x, Na - z_y) + \frac{z_x}{a} \left( N - \frac{z_y}{a} \right) A_2(Na - z_x, z_y) \rho_2(Na - z_x, z_y) + \frac{z_x}{a} \frac{z_y}{a} A_2(Na - z_x, Na - z_y) \rho_2(Na - z_x, Na - z_y) \right\}. \tag{2.20}
\end{aligned}$$

If periodic boundary conditions are used,  $\rho_2$  satisfies the same periodicity, so that  $|\phi(\vec{k})|^2 \rho_2$  is given by

$$\begin{aligned}
|\phi(\vec{k})|^2 \rho_2(\vec{z}) &= N^3 \mathcal{F}^{-1}[\vec{z}, \vec{k}]\{\langle\langle I(\vec{k}) \rangle\rangle\} \Big/ \left[ \left( N - \frac{z_x}{a} \right) \left( N - \frac{z_y}{a} \right) A_2(z_x, z_y) + \left( N - \frac{z_x}{a} \right) \frac{z_y}{a} A_2(z_x, Na - z_y) \right. \\
&\quad \left. + \frac{z_x}{a} \left( N - \frac{z_y}{a} \right) A_2(Na - z_x, z_y) + \frac{z_x}{a} \frac{z_y}{a} A_2(Na - z_x, Na - z_y) \right]. \tag{2.21}
\end{aligned}$$

The second term of  $\langle\langle I^2(\vec{k}) \rangle\rangle_L$  [Eq. (2.12)] can now be calculated by substituting  $|\phi(\vec{k})|^2 \rho_2$  in the second term of Eq. (2.11). Although the function  $A_2$  in the denominator does have zero points, all four of the  $A_2$ 's are never simultaneously zero and there is no difficulty.

This completes the approximate calculation of  $\langle\langle I^2(\vec{k}) \rangle\rangle_H$

from quantities derivable from a single TEM image. We call the approximate HSC calculated in this way the eHSC.

### III. PRACTICAL PROCEDURE TO OBTAIN THE eHSC

In this section we summarize the practical procedure to calculate the eHSC from a single experimentally obtained

TEM image. Ensemble averages are assumed to be replaced by spatial averages in the practical procedure.

(1) Sample the TEM dark-field image intensities  $|U(\vec{k}, \vec{j}a)|^2$  at the sampling lattice points  $\{\vec{j}a|j_\alpha = 1, 2, \dots, N (\alpha = x, y)\}$  of the  $N \times N$  square lattice.  $\vec{k}$  takes the values  $\{2\pi\vec{j}/(Na)|j_\alpha = 1, 2, \dots, N (\alpha = x, y)\}$ .

(2) Calculate  $\langle\langle I(\vec{k}) \rangle\rangle$  and  $\langle\langle I^2(\vec{k}) \rangle\rangle$  using the following formulas:

$$\langle\langle I(\vec{k}) \rangle\rangle = \frac{1}{N^2} \sum_{\vec{j}} |U(\vec{k}, \vec{j}a)|^2, \quad (3.1)$$

$$\langle\langle I^2(\vec{k}) \rangle\rangle = \frac{1}{N^2} \sum_{\vec{j}} |U(\vec{k}, \vec{j}a)|^4. \quad (3.2)$$

(3) Calculate the three terms of  $\langle\langle I^2(\vec{k}) \rangle\rangle_L$  [cf., Eq. (3.12)] as follows.

(a) The first term in  $\langle\langle I^2(\vec{k}) \rangle\rangle_L$  is given by

$$\frac{1}{N^2} \sum_{\vec{j}'} 2 \left\{ \frac{1}{N^2} \sum_{\vec{j}} |U(\vec{k}, \vec{j}a)|^2 \right\}^2 = 2 \langle\langle I(\vec{k}) \rangle\rangle^2. \quad (3.3)$$

(b) The second term in  $\langle\langle I^2(\vec{k}) \rangle\rangle_L$  is calculated in the following three steps.

(i) First, discrete inverse Fourier transform the  $\langle\langle I(\vec{k}) \rangle\rangle$  as follows:

$$\mathcal{F}^{-1}[z, \vec{k}] \{ \langle\langle I(\vec{k}) \rangle\rangle \} = \frac{1}{N} \sum_{\vec{k}_x=1}^N \sum_{\vec{k}_y=1}^N \langle\langle I(\vec{k}) \rangle\rangle e^{-i\vec{k} \cdot \vec{z}}, \quad (3.4)$$

where the  $\alpha$  component of  $\vec{z}$  takes  $a, 2a, \dots, Na$  and  $k_\alpha = 2\pi\vec{k}_\alpha/(Na)$  ( $\vec{k}_\alpha = 1, 2, \dots, N$ ).

(ii) Next, use Eq. (2.21) to compute  $|\phi(\vec{k})|^2 \rho_2$ . That is, use the following formula reproduced for convenience:

$$\begin{aligned} |\phi(\vec{k})|^2 \rho_2(\vec{z}) &= N^3 \times \mathcal{F}^{-1}[z, \vec{k}] \\ &\times \{ \langle\langle I(\vec{k}) \rangle\rangle \} / \left[ \left( N - \frac{z_x}{a} \right) \left( N - \frac{z_y}{a} \right) A_2(z_x, z_y) \right. \\ &+ \left( N - \frac{z_x}{a} \right) \frac{z_y}{a} A_2(z_x, Na - z_y) \\ &+ \frac{z_x}{a} \left( N - \frac{z_y}{a} \right) A_2(Na - z_x, z_y) \\ &\left. + \frac{z_x}{a} \frac{z_y}{a} A_2(Na - z_x, Na - z_y) \right]. \quad (3.5) \end{aligned}$$

(iii) Finally, substitute that into the second term in  $\langle\langle I^2(\vec{k}) \rangle\rangle_L$  to yield

$$\frac{1}{N^2} \sum_{\vec{j}} |G(\vec{j}a, \vec{k})|^2, \quad (3.6)$$

where

$$\begin{aligned} G(\vec{j}a, \vec{k}) &= \mathcal{F}[\vec{n}a, \vec{k}] \left\{ \sum_{m_x=1}^{n_x-1} \sum_{m_y=1}^{n_y-1} A(\vec{j}a - \vec{m}a) A(\vec{j}a - \vec{n}a + \vec{m}a) |\phi(\vec{k})|^2 \rho_2(2\vec{m}a - \vec{n}a) (1 - \delta_{n_x,1}) (1 - \delta_{n_y,1}) \right\} \\ &+ \mathcal{F}[\vec{n}a, \vec{k}] \left\{ \sum_{m_x=1}^{n_x-1} \sum_{m_y=0}^{N-n_y} A((j_x - m_x)a, (j_y - m_y - n_y)a) A((j_x + m_x - n_x)a, (j_y + m_y - N)a) \right. \\ &\times \left. |\phi(\vec{k})|^2 \rho_2((2m_x - n_x)a, (2m_y + n_y - N)a) (1 - \delta_{n_x,1}) \right\} \\ &+ \mathcal{F}[\vec{n}a, \vec{k}] \left\{ \sum_{m_x=0}^{N-n_x} \sum_{m_y=1}^{n_y-1} A((j_x - m_x - n_x)a, (j_y - m_y)a) A((j_x + m_x - N)a, (j_y + m_y - n_y)a) \right. \\ &\times \left. |\phi(\vec{k})|^2 \rho_2((2m_x + n_x - N)a, (2m_y - n_y)a) (1 - \delta_{n_y,1}) \right\} \\ &+ \mathcal{F}[\vec{n}a, \vec{k}] \left\{ \sum_{m_x=0}^{N-n_x} \sum_{m_y=0}^{N-n_y} A(\vec{j}a - \vec{m}a - \vec{n}a) A(\vec{j}a - \vec{m}a - Na\hat{x} - Na\hat{y}) |\phi(\vec{k})|^2 \rho_2(2\vec{m}a + \vec{n}a - Na\hat{x} - Na\hat{y}) \right\}. \quad (3.7) \end{aligned}$$

Discrete Fourier transform  $\mathcal{F}[\vec{n}a, \vec{k}]\{\dots\}$  is defined by Eq. (2.16) and  $\hat{x}$  and  $\hat{y}$  are unit vectors parallel to  $x$  and  $y$  axes, respectively.

(c) Calculate the third term in  $\langle\langle I^2(\vec{k}) \rangle\rangle_L$  from the spatial average density  $\bar{\rho}_1$  and the atomic scattering factor  $\phi(\vec{k})$ ,

$$\begin{aligned} & -\frac{2}{N^2} \sum_{\vec{j}} \left| \frac{\phi(\vec{k})}{N^{1/2}} \sum_{\vec{j}_1} A(\vec{j}a - \vec{j}_1a) \bar{\rho}_1 e^{i\vec{k} \cdot \vec{j}_1a} \right|^4 \\ & = -2(|\phi(\vec{k})| \bar{\rho}_1)^4 \sum_{\vec{j}} |\mathcal{F}[\vec{j}_1a, \vec{k}]\{A(\vec{j}a - \vec{j}_1a)\}|^4 \end{aligned} \quad (3.8)$$

( $\bar{\rho}_1$  is the spatial average density because spatial averages have replaced ensemble averages).

(4) Compute  $\langle\langle I^2(\vec{k}) \rangle\rangle_L$  as the sum of Eqs. (3.3), (3.6), and (3.8). Obtain  $\langle\langle I^2(\vec{k}) \rangle\rangle_H$  by subtracting  $\langle\langle I^2(\vec{k}) \rangle\rangle_L$  from  $\langle\langle I^2(\vec{k}) \rangle\rangle$  [Eq. (3.2)].

(5) Finally, obtain the eHSC by dividing  $\langle\langle I^2(\vec{k}) \rangle\rangle_H$  by  $\langle\langle I^2(\vec{k}) \rangle\rangle_L$ .

The procedure to calculate the eHSC may appear complicated, but the computational cost except for the Fourier transformation is not much larger than that for the NSV. Therefore, the eHSC should be accessible experimentally without difficulty. As is demonstrated in the next section, the extra computation cost of the Fourier transformation, which is not very heavy with the aid of the fast Fourier transformation algorithm, is worth paying.

#### IV. NUMERICAL DEMONSTRATION

To demonstrate the detecting power of the eHSC, we need two samples with known subtle structural differences. It is almost impossible to use actual samples to this end, so here we give a detailed numerical demonstration of the sensitivity of the eHSC and the NSV. We investigate the behavior of these quantities as a function of the amount of randomness, the objective aperture reciprocal radius  $Q$ , and the degree of simulated experimental noise. The HSC is also studied as a comparison with the eHSC and NSV, although the HSC is not obtainable from a single TEM image.

##### A. Model system

In order to investigate the sensitivity of the eHSC, NSV, and HSC to subtle spatial structural changes, we consider simple two-dimensional numerical specimens that are subjected to small random structural perturbations. There are 16 atoms on a  $4 \times 4$  square lattice in each specimen. This may be considered to be the lattice unit cell of some material. The position of one randomly selected atom is displaced slightly in a random direction from the regular lattice point with the remaining atoms unchanged. The absolute value of the displacement is  $D \times l_0$ , where  $l_0$  is the lattice constant of the  $4 \times 4$  square lattice and we chose five different  $D$ ; 0.025, 0.05, 0.075, 0.1, and 0.2. We assume  $l_0 = 2.5$  (Å), which is nearly equal to the average distance between nearest-neighbor atoms in metal silicon. The direction of the displacement vector can assume any direction ran-

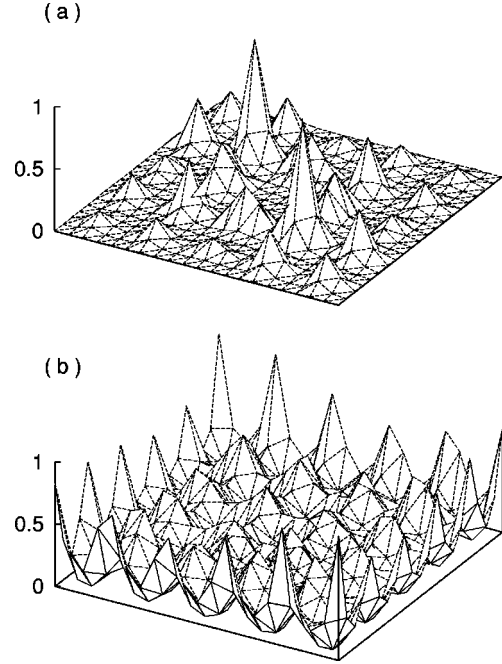


FIG. 1. Bird's-eye-view plots of (a) eHSC and (b) NSV for  $Q = 0.1 \times 2\pi$  and  $D = 0.05$  on  $-2\pi \leq k_x, k_y \leq 2\pi$ .

domly in a two-dimensional specimen. Since an atom has a finite radius, the atomic density function  $\psi$  is well approximated by the sum of 16 Gaussian profiles localized around the atom positions:

$$\psi(\vec{r}) = \sum_{j=1}^{16} \frac{1}{\pi w^2} \exp\left\{-\frac{|\vec{r} - \vec{r}_j|^2}{w^2}\right\}, \quad (4.1)$$

where  $\vec{r}_j$  is the position of the center of the  $j$ th atom and  $w = 0.5$  (Å) is assumed to be the Fourier transform of the scattering factor half-width observed by diffraction experiments on a silicon crystal. The Debye-Waller factor is not considered in our model, because it is the higher-order correction to TEM experiments.

For each value of  $D$ , ten numerical specimens are prepared in order to make an ensemble of structures. We use the same random number sequence to make the ten specimens for each  $D$ . Therefore, differences among sets of ensemble depend only on the difference of  $D$ . The specimen is sampled on the  $N \times N$  ( $N = 64$ ) sampling lattice points for numerical calculation. Therefore, the sampling lattice spacing  $a$  is  $4l_0/L = 10/64$  (Å). The periodic-boundary condition is used for each specimen.

We choose eight radii of the objective aperture in reciprocal space,  $Q$  between  $0.1 \times 2\pi$  and  $0.01 \times 2\pi$  (Å<sup>-1</sup>). The eHSC, NSV, and HSC are calculated for each set of  $(D, Q)$ .

$\langle\langle I \rangle\rangle$  and  $\langle\langle I^2 \rangle\rangle$  are very simple with a few sharp peaks around the origin of the  $\vec{k}$  space and without significant dependence on  $(D, Q)$ . They are not considered further in this paper.

##### B. eHSC vs NSV

Figures 1(a) and 1(b) show a bird's-eye view of the eHSC and NSV on the two-dimensional  $\vec{k}$  space. The center of the

square in these figures is the origin of the  $\vec{k}$  space. We show the region  $-2\pi \leq k_x, k_y \leq 2\pi (\text{\AA}^{-1})$  because the maximum value of  $|\vec{k}|$  accessible to experiment is approximately  $0.75 \times 2\pi (\text{\AA}^{-1})$ .<sup>2</sup> In order to illustrate differences between the eHSC and NSV, these quantities are normalized so that the difference between the maximum and minimum value is unity. In general, simple patterns are found in eHSC, while the NSV has very complex patterns.

The eHSC grows with the increase of  $D$ . The NSV changes in a complicated way, showing many small peaks in the whole  $\vec{k}$  region. Consequently, the eHSC appears to change with  $D$  more systematically than the NSV. This may be due to the fact that the patterns in the eHSC for an almost regular lattice ( $D \approx 0$ ) are much smaller than those for  $D \neq 0$ , while the patterns in the NSV for  $D = 0$  are similar to those for  $D \neq 0$ .

In order to extract the  $D$  dependence we plot for each quantity the difference between  $D = 0.075, 0.2$  and  $D = 0.05$ . Figures 2(a) and 2(b) show eHSC ( $D = 0.075, 0.2$ ) - eHSC ( $D = 0.05$ ). Figures 2(c) and 2(d) show the same thing for the NSV. As the difference in  $D$  becomes larger, both the number and the heights of the peaks in both quantities increase. Thus, we may conclude that both the eHSC and NSV can detect subtle random changes occurring in real space structures, although the eHSC shows the changes more clearly.

The  $Q$  dependence of the eHSC and NSV are illustrated in Figs. 3(a)–3(d) in a similar way. Figures 3(a) and 3(b) show eHSC ( $Q = 0.075 \times 2\pi, 0.025 \times 2\pi$ ) - eHSC ( $Q = 0.1 \times 2\pi$ ). Figures 3(c) and 3(d) show the same thing for the NSV. The eHSC and NSV grow larger with the decrease of  $Q$ , because the range of correlations that is detected by the NSV and HSC increases with the decrease of  $Q$  by definition. In other words, the sensitivity of both quantities to subtle structural changes is enhanced as  $Q$  becomes smaller. Therefore, although higher-order spatial correlations are not so important in our model, the capability to detect medium-range spatial correlation by both NSV and eHSC is expected to be enhanced by the decrease of  $Q$ .

### C. Stability of the eHSC and NSV against noise

We have also investigated the stability of the eHSC and NSV against simulated experimental noise. Since the dark-field-image intensity  $|U(\vec{k}, \vec{r})|^2$  is observed directly by TEM experiments, it is natural to add noise to  $|U(\vec{k}, \vec{r})|^2$ . Uniform random noise in  $[-A_{mp}, A_{mp}]$  is added to  $|U(\vec{k}, \vec{r})|^2$  and the eHSC and NSV are calculated for various values of  $A_{mp}$ . The eHSC and NSV become unstable against noise beyond some  $A_{mp}$  which is denoted by  $A_{mp}^c$ . With  $Q = 0.1 \times \pi$  and  $D = 0.1$ ,  $A_{mp}^c$  for the eHSC lies between  $2 \times 10^{-2}$  and  $7 \times 10^{-2}$ , as can be seen by noting the formation of the large features at the corners of  $\vec{k}$  space with the increase of noise amplitudes in Figs. 4(a) and 4(b).  $A_{mp}^c$  for the NSV is between  $10^{-3}$  and  $2 \times 10^{-3}$ , as seen in Figs. 4(c) and 4(d). Hence, the eHSC is significantly more stable against artificial noise than the NSV.

We have found the same tendency for other sets  $(Q, D)$ . For  $(Q, D) = (0.5 \times 2\pi, 0.1)$ ,  $A_{mp}^c$  for the eHSC is between  $10^{-2}$  and  $2 \times 10^{-2}$ , while that for the NSV is between  $10^{-4}$

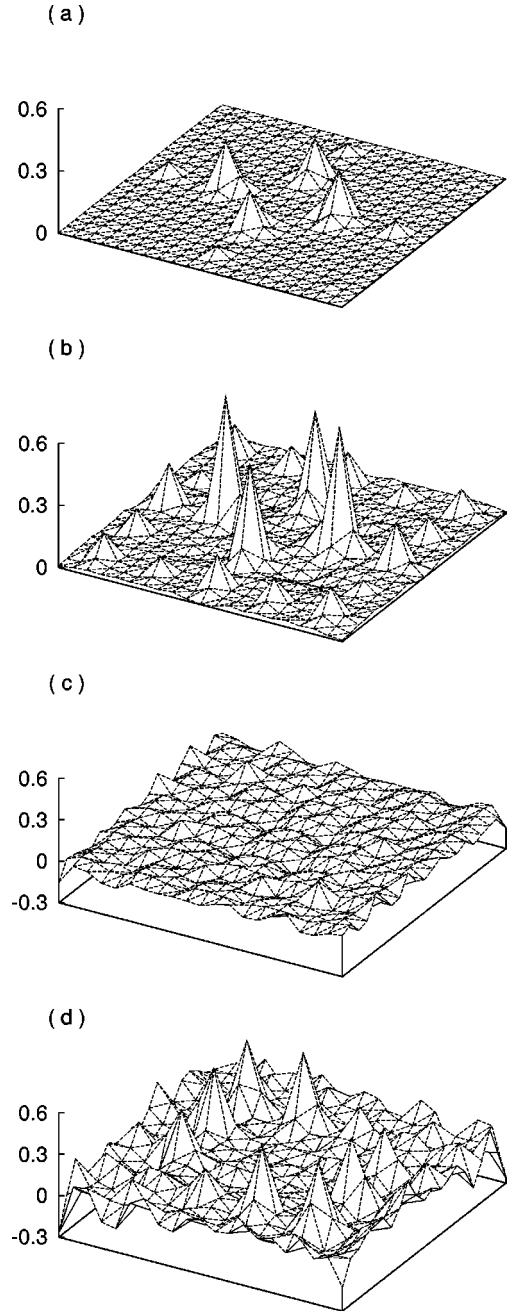


FIG. 2.  $D$  dependence of the eHSC and NSV for  $Q = 0.1 \times 2\pi$  on  $-2\pi \leq k_x, k_y \leq 2\pi$ . (a) Difference between eHSC for  $D = 0.075$  and eHSC for  $D = 0.05$ . (b) Difference between eHSC for  $D = 0.2$  and eHSC for  $D = 0.05$ . (c) Difference between NSV for  $D = 0.075$  and NSV for  $D = 0.05$ . (d) Difference between NSV for  $D = 0.2$  and NSV for  $D = 0.05$ .

and  $10^{-3}$ .  $A_{mp}^c$  for both quantities becomes smaller with the decreasing  $Q$ , because the sensitivity of both quantities to subtle structural changes becomes better with the decreasing  $Q$ . However,  $A_{mp}^c$  for the NSV is much smaller than that for the eHSC.

In the case of  $(Q, D) = (0.1 \times 2\pi, 0.05)$ ,  $A_{mp}^c$  for the eHSC is between  $4 \times 10^{-2}$  and  $0.1$ . That for the NSV is between  $10^{-4}$  and  $10^{-3}$ . Although  $A_{mp}^c$  for the eHSC is almost equal to that for  $(Q, D) = (0.1 \times 2\pi, 0.1)$ ,  $A_{mp}^c$  for the NSV becomes smaller as  $D$  becomes smaller.

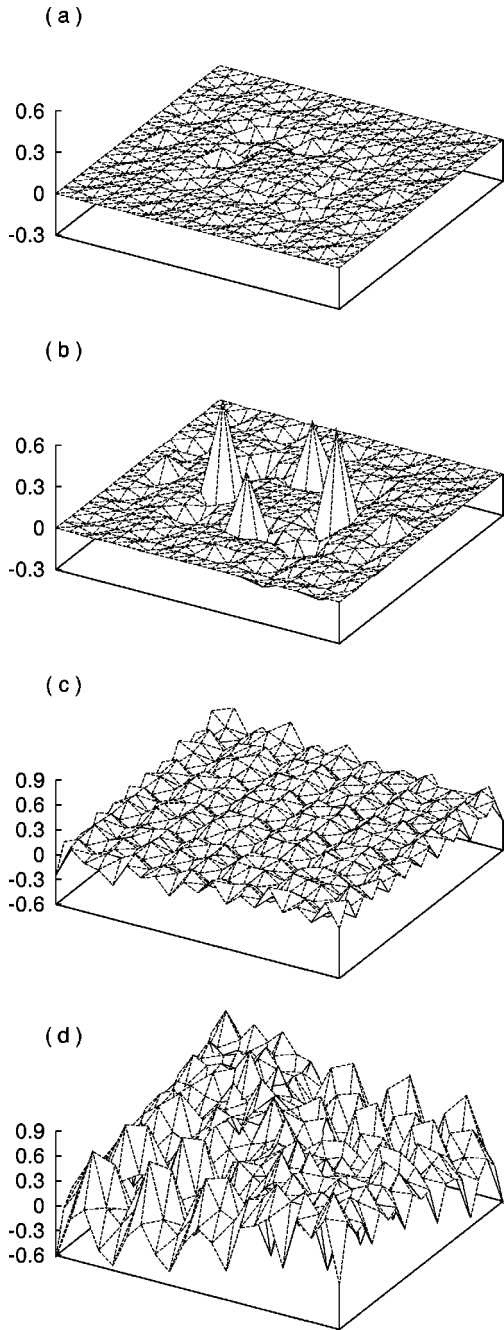


FIG. 3.  $Q$  dependence of the eHSC and NSV for  $D=0.05$  on  $-2\pi \leq k_x, k_y \leq 2\pi$ . (a) Difference between eHSC for  $Q=0.075 \times 2\pi$  and eHSC for  $Q=0.1 \times 2\pi$ . (b) Difference between eHSC for  $Q=0.025 \times 2\pi$  and eHSC for  $Q=0.1 \times 2\pi$ . (c) Difference between NSV for  $Q=0.075 \times 2\pi$  and NSV for  $Q=0.1 \times 2\pi$ . (d) Difference between NSV for  $Q=0.025 \times 2\pi$  and NSV for  $Q=0.1 \times 2\pi$ .

In general, the improved stability of the eHSC against noise occurs because it is more dominated by higher-order correlation contributions than the NSV. The noise is not spatially correlated and as a result effects primarily the lower-order correlation functions.

#### D. HSC vs eHSC and NSV

The HSC is calculated directly from Eqs. (2.10), (2.12), and (2.13), that is, without the assumption, Eq. (2.14). To

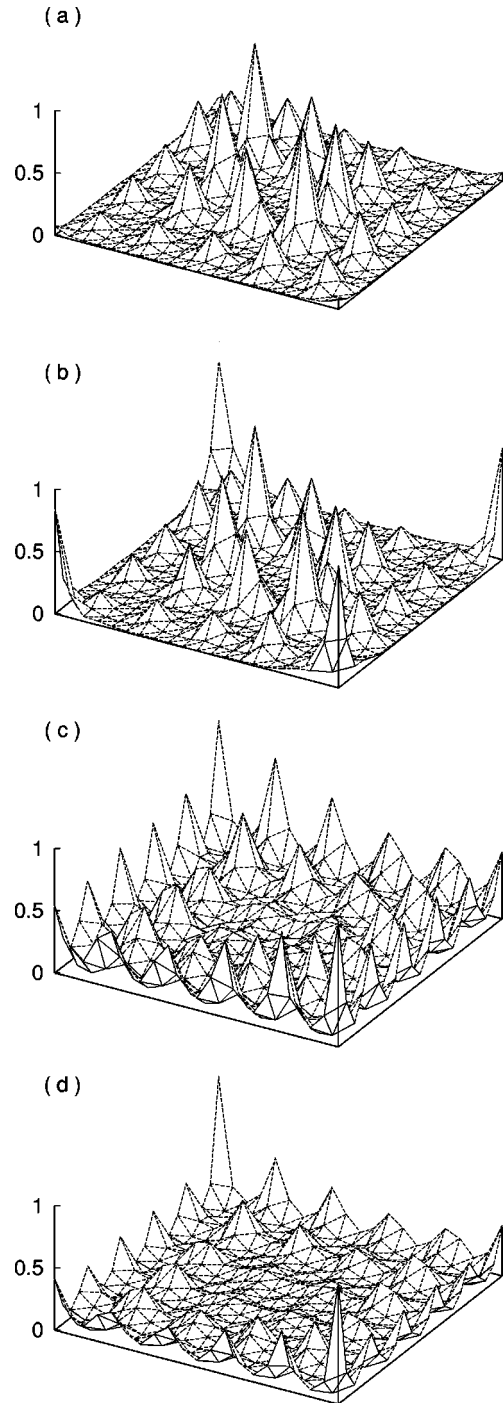


FIG. 4. Noise stability of the eHSC and NSV for  $Q=0.1 \times 2\pi$  and for  $D=0.1$  on  $-2\pi \leq k_x, k_y \leq 2\pi$ . (a) eHSC for  $A_{mp}=2 \times 10^{-2}$ . (b) eHSC for  $A_{mp}=7 \times 10^{-2}$ . (c) NSV for  $A_{mp}=10^{-3}$ . (d) NSV for  $A_{mp}=2 \times 10^{-3}$ .

compare the  $D$  dependence of the HSC with that of the eHSC, we follow the same method used in Figs. 2(a) and 2(b), as shown in Figs. 5(a) and 5(b). The HSC also grows with the increase of  $D$ . The change in both number and heights of peaks in the HSC with  $D$  is larger than that of the eHSC. Therefore, the HSC appears to be an even better quantity to detect subtle spatial randomness than the eHSC. It is not, however, currently experimentally accessible.

The  $Q$  dependence of the HSC is illustrated in Figs. 5(c) and 5(d) in the same way as in Figs. 3(a) and 3(b). We

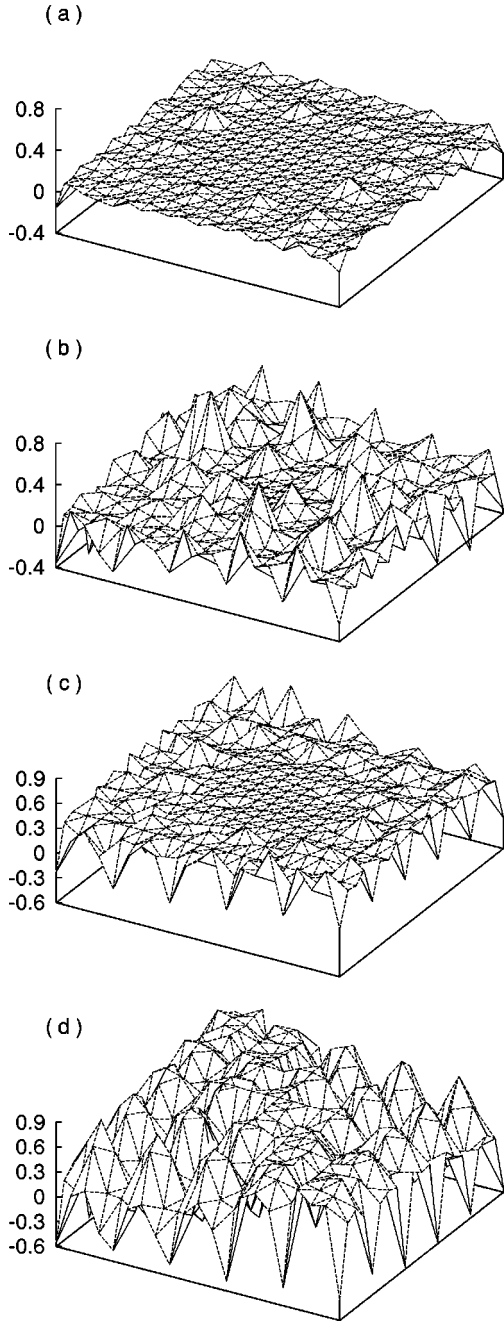


FIG. 5. Dependence of HSC on  $D$  and  $Q$  on the reciprocal space  $-2\pi \leq k_x, k_y \leq 2\pi$ .  $D$  dependence of the HSC for  $Q = 0.1 \times 2\pi$  is shown in (a) and (b).  $Q$  dependence of the HSC for  $D = 0.05$  is shown in (c) and (d). (a) Difference between HSC for  $D = 0.075$  and HSC for  $D = 0.05$ . (b) Difference between HSC for  $D = 0.2$  and HSC for  $D = 0.05$ . (c) Difference between HSC for  $Q = 0.075 \times 2\pi$  and HSC for  $Q = 0.1 \times 2\pi$ . (d) Difference between HSC for  $Q = 0.025 \times 2\pi$  and HSC for  $Q = 0.1 \times 2\pi$ .

realize that the HSC is the most sensitive to the change of  $Q$  among the eHSC, HSC, and NSV. The better sensitivity of the HSC to both  $D$  and  $Q$  is reasonable given its exact removal of the lower-order correlation functions.

#### E. Sensitivity of the eHSC and NSV to change in a random pattern

All the results discussed so far have been for a completely regular underlying structure subject to a small perturbation.

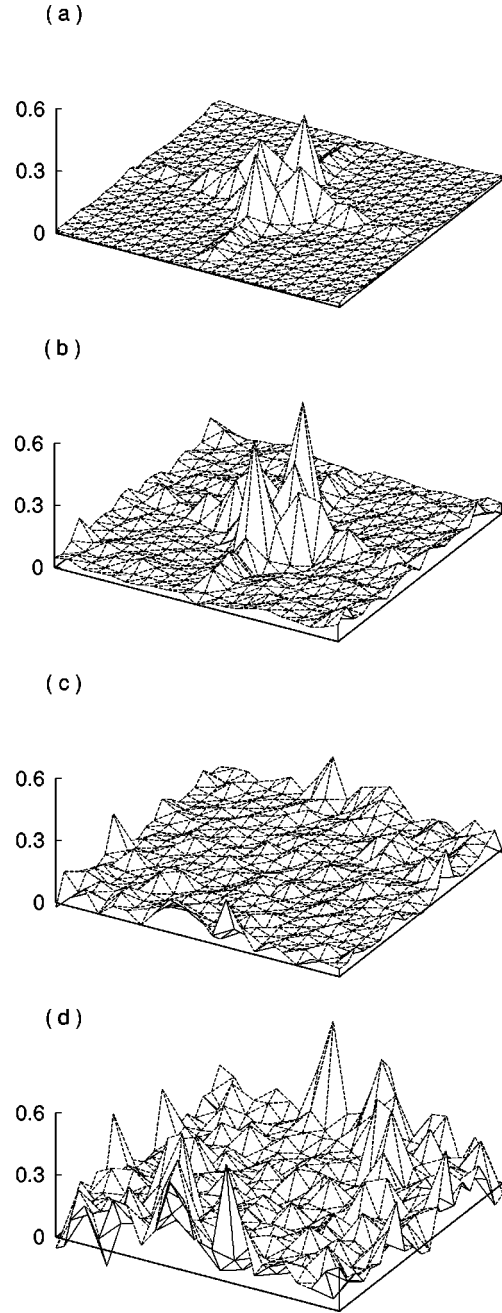


FIG. 6.  $D$  dependence of the HSC and NSV for  $Q = 0.1 \times 2\pi$  on  $-2\pi \leq k_x, k_y \leq 2\pi$  in the case of random underlying structure. (a) Difference between eHSC for  $D = 0.1$  and eHSC for  $D = 0.05$ . (b) Difference between eHSC for  $D = 0.2$  and eHSC for  $D = 0.05$ . (c) Difference between NSV for  $D = 0.1$  and NSV for  $D = 0.05$ . (d) Difference between NSV for  $D = 0.2$  and NSV for  $D = 0.05$ .

To check that the sensitivity of the eHSC or NSV remains intact for irregular structures we performed a similar displacement detection simulation for a random structure prepared by displacing every atom from the regular lattice position by  $0.3 \times l_0$  in a random direction. To this basic irregular configuration of atoms, a single atom is randomly chosen and slightly displaced further (just as in the regular lattice simulation above). The displacement is  $D \times l_0$  with  $D = 0.05, 0.1$ , and  $0.2$ . In Figs. 6(a) and (b), the eHSC for the random pattern are shown for  $D = 0.1$  and  $D = 0.2$  relative to that for  $D = 0.05$  [in the same way as in Figs. 2(a) and 2(b)].

In Figs. 6(c) and 6(d), the results for the NSV are shown. The degree of structural changes in these quantities is similar to that in simulations using the regular sample. Thus, we conclude that the ability of the eHSC and NSV to detect subtle changes in a structure is independent of the underlying structure.

## V. SUMMARY AND DISCUSSION

We have suggested the empirical higher-order speckle cumulant, an improvement to the normalized speckle variance introduced by Treacy and Gibson,<sup>1</sup> which better detects subtle changes in spatial structures than the two-body correlation function or the form factor. The newly proposed quantity, like the NSV, can be calculated solely from a series of dark-field TEM images.

We have numerically demonstrated the following.

(i) Patterns in both the eHSC and NSV grow with an increase in the random perturbation applied to both an ordered and disordered numerical specimen. Therefore, both the eHSC and NSV are much better quantities to detect subtle random structure changes than the two-body correlation function or the form factor. This is primarily because both the eHSC and the NSV contain contributions from higher-order correlation functions, although they also re-

move the large  $\vec{k}=0$  features found in the average diffracted intensity.

(ii) The eHSC is more stable against noise than the NSV, so that the fine structures of the former are more significant than those of the latter. This is because the noise primarily contributes to lower-order correlations, which are well subtracted in the eHSC.

We also demonstrated that if we could remove the effect of lower-order correlations exactly as in the HSC, the result should be much more sensitive to both the magnitude of the displacement  $D$  and the resolution  $Q$  than the eHSC and NSV. Finding experimentally reliable methods to calculate the HSC is one possible extension of this work.

The other important remaining problem is to understand the correspondence between the actual structure and the eHSC. This is difficult because we do not have a good intuitive grasp of the underlying higher-order correlation functions. We hope to develop such an understanding in the future.

## ACKNOWLEDGMENTS

This work was, in part, supported by National Science Foundation Grants No. DMR-93-14938 and No. DMR-97-03906.

<sup>1</sup>M.M.J. Treacy and J.M. Gibson, *Acta Crystallogr., Sect. A: Found. Crystallogr.* **52**, 212 (1996).

<sup>2</sup>J.M. Gibson and M.M.J. Treacy, *Phys. Rev. Lett.* **78**, 1074 (1997).

<sup>3</sup>M.M.J. Treacy, J.M. Gibson, and P.J. Keblinski, *J. Non-Cryst. Solids* **231**, 99 (1998).

<sup>4</sup>S. Brauer, G.B. Stephenson, M. Sutton, R. Brüning, E. Dufresne, S.G.J. Mochrie, G. Grübel, J. Als-Nielsen, and D.L. Abernathy, *Phys. Rev. Lett.* **74**, 2010 (1995).

<sup>5</sup>S.G.J. Mochrie, A.M. Mayers, A.R. Sandy, M. Sutton, S. Brauer, G.B. Stephenson, D.L. Abernathy, and G. Grübel, *Phys. Rev. Lett.* **78**, 1275 (1997).

<sup>6</sup>S.B. Dierker, R.M. Fleming, I.K. Robinson, and L. Berman, *Phys. Rev. Lett.* **75**, 449 (1995).

<sup>7</sup>T. Thurn-Albrecht, W. Steffen, A. Patkowski, G. Meier, E.W. Fisher, G. Grübel, and D.L. Abernathy, *Phys. Rev. Lett.* **77**, 5437 (1996).

<sup>8</sup>G. Brown, P.A. Rikvold, and M. Grant, *Physica A* **239**, 263 (1997).

<sup>9</sup>M.M.J. Treacy and J.M. Gibson, *Ultramicroscopy* **52**, 31 (1993).

<sup>10</sup>R. Abe, *Statistical Mechanics* (University of Tokyo Press, Tokyo, 1966) (in Japanese); L.E. Reichl, *A Modern Course in Statistical Physics* (Wiley, New York, 1997).